Acta Neurochir (Wien) (2004) 146: 1211–1220
DOI 10.1007/s00701-004-0352-y

Acta Neurochirurgica
Printed in Austria

Technical Assessment

Real-time integration of ultrasound into neuronavigation: technical accuracy using a light-emitting-diode-based navigation system

A. Jödicke, T. Springer, and **D.-K. Böker**

Department of Neurosurgery, University Medical Centre, Justus-Liebig-Universität, Giessen, Germany

Published online September 20, 2004

Summary

Background. In brain surgery, intraoperative brain deformation is the major source of postimaging inaccuracy of neuronavigation. For intraoperative imaging of brain deformation, we developed a platform for the integration of ultrasound imaging into a navigation system.

Method. A commercially available ultrasound system was linked to a light-emitting-diode- (LED) based neuronavigation system via rigid fixation of a position localiser to the ultrasound probe and ultrasound image transfer into the navigation system via a S-VHS port. Since the position of the ultrasound image co-ordinate system is not readily defined within the navigation reference co-ordinate system (REF CS), a transformation which links both co-ordinate systems has to be defined by a calibration procedure. Calibration of the ultrasound probe within the REF CS was performed via a cross-wire phantom. The phantom target was defined within the navigation co-ordinate system (by pointer under microscopic control) and imaged by ultrasound. Ultrasound presets were optimised (digital beam focusing, gain intensity) to attain a small echoic target for manual target definition. The transformation was derived from 150 ultrasound measures and iteration. Accuracy was calculated as mean linear error (LE; in X_{REF}, Y_{REF}, or Z_{REF} direction), overall mean LE (linear errors of all axes X_{REF} to Z_{REF}) and Euclidean error (EE; vectorial distance from the physical target).

Findings. Optimised ultrasound presets (8 MHz frequency, digital beam focusing, 20% gain intensity) enabled a low interobserver error (mean: 0.5 mm, SD: 0.28) for target definition within the 2-D ultrasound image. Mean accuracy of pointer-based physical target definition in the REF CS was 0.7 mm (RMSE; SD: 0.23 mm). For navigated ultrasound, the overall mean LE was 0.43 mm (SD: 1.36 mm; 95%CL: 3.13 mm) with a mean EE of 2.26 mm (SD: 0.97 mm; 95%CL: 4.21 mm).

Interpretation. Using a single target cross-wire phantom, a highly accurate integration of ultrasound imaging into neuronavigation was achieved. The phantom accuracy of integration lies within the range of application accuracy of navigation systems and warrants clinical studies.

Keywords: Ultrasound; image-guided surgery; intraoperative imaging; neuronavigation; brain distortion.

Introduction

Intraoperative image guidance based on preoperative imaging is prone to inaccuracies due to brain deformation [6, 11, 18, 20]. Intraoperative imaging is the main approach to overcome this source of inaccuracy. Intraoperative MR imaging [1, 22] involves considerable costs. Intraoperative CT inherits the burden of radiation and limits unrestrained intraoperative use. Both techniques require considerable reorganization of the patients positioning, the operation room equipment and the medical staff.

Intraoperative ultrasound correlated to image guided surgery was introduced by Koivukangas in 1986 [14]. The use of intraoperative 3-D-ultrasound as a basis of adjustment for brain deformation was initially proposed by some research groups [3, 8, 10, 12, 13, 21]. Calibration accuracy of the integration of ultrasound into neuronavigation systems has been reported by some authors [9, 15, 17, 21], however, most have focussed on preliminary clinical aspects. Accurate calibration, however, is of utmost importance for precise image overlay with MR imaging and 3-D image reconstruction especially for supplementary use in clinical neuronavigation [19]. This paper describes the technique and accuracies of ultrasound integration into a LED-based neuronavigation system.

Materials and methods

Technical equipment and coordinate systems (CS)

We used a LED-based neuronavigation device (SMN, Carl Zeiss Inc., Oberkochen, Germany; STP4.x software, Leibinger Inc., Freiburg,

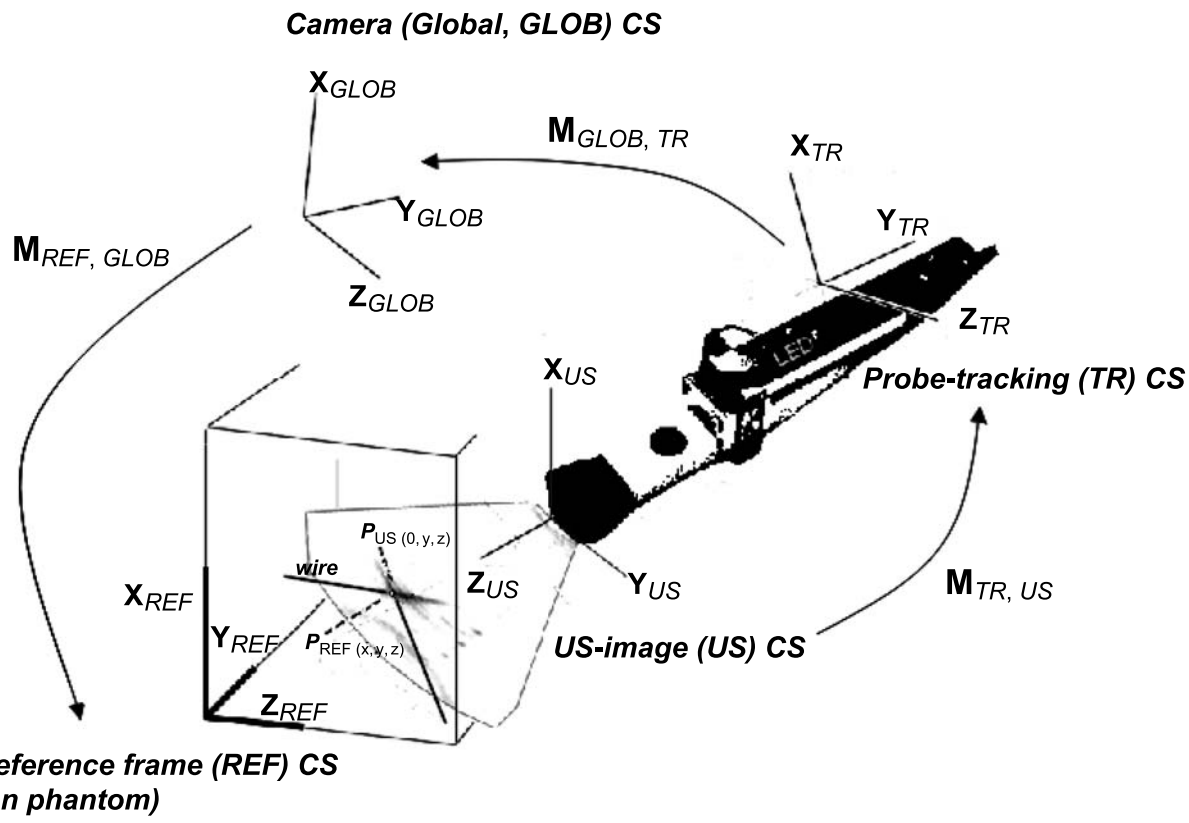

Fig. 1. Definition of the co-ordinate systems (*CS*) used for calibration. Target point ***P*** is defined within the reference frame co-ordinate system (*REF CS,* $\boldsymbol{P}_{REF}$) and imaged in the ultrasound co-ordinate system (*US CS,* $\boldsymbol{P}_{US}$). The US CS is related to the ultrasound probe, which is defined in a tracking device co-ordinate system (*TR CS*) by a LED-emitter. This relation of US CS to TR CS is to be determined by the calibration process by calculating the appropriate transformation $M_{TR,US}$. REF CS and TR CS are linked by the camera system as a global co-ordinate system (*GLOB CS*). According transformations (M) are depicted

Germany) for navigational planning and intraoperative guidance. The co-ordinate system (CS) of the navigation was defined by a reference frame (REF CS) attached to the calibration phantom. A tracking device co-ordinate system (TR CS) was related to the REF CS by the navigation camera system serving as a global coordinate system (GLOB CS, see Fig. 1).

For intraoperative ultrasound examinations a widely used ultrasound system (2002 panther, B&K Medical, Gentofte, Denmark) was employed. Probes 8563 (12 mm phased array probe for key hole approaches) and 8562 (curved array probe for resection control in microsurgical craniotomy cases) were chosen for the integration into neuronavigation. An optical emitter rod (6 LED's; Carl Zeiss Inc., Oberkochen, Germany) was rigidly attached to each ultrasound probe allowing the surgeon to hold the probe like a pencil. This tracking device defined the localization and orientation of the ultrasound probe.

Phantom

A cross-wire phantom was chosen for calibration. 0.2 mm nylon threads were fixed in a plexiglas water tank (20×20 cm) forming a cross, serving as the physical target. Ten titanium screws were fixed to the tank for registration of the phantom. The reference frame was rigidly affixed to the phantom and frame axes where aligned to the principle axes of the phantom. Therefore, all phantom coordinates where measured within the reference frame coordinate system (REF CS). Since a commercial navigation system was used, image data must be registered to the phantom for tracking the ultrasound probe within REF CS. The phantom was scanned by CT with 1 mm slices (non-helical CT; GE Hi Speed, 0.43 mm pixel size) for registration.

Probe calibration

Localization of the physical target using a tracked pointer

After phantom registration, the position of the target point ***P*** within the REF CS ($\boldsymbol{P}_{REF}$; Fig. 1) as defined by the crossed threads was determined by using the pointer (mean of ten data samples under microscopical assistance). Errors of fiducial localization and target localisation within the REF CS were calculated as root mean square error (RMSE).

Ultrasound settings and manual identification of target points in ultrasound image

To achieve highest accuracy in identification of the ultrasound target, image clarity of the ultrasound image was evaluated by two observers using a ten tiered arbitrary scale (least to best clarity, 0–10 units). Digital beam focusing and intensity of gain were ranked for its influence on image clarity, i.e. sharpness of the target edges, thus defining the presets for the calibration procedure. Target co-ordinates were determined within each 2-D ultrasound image (tagged image format, 898×898 pixel; Fig. 2)

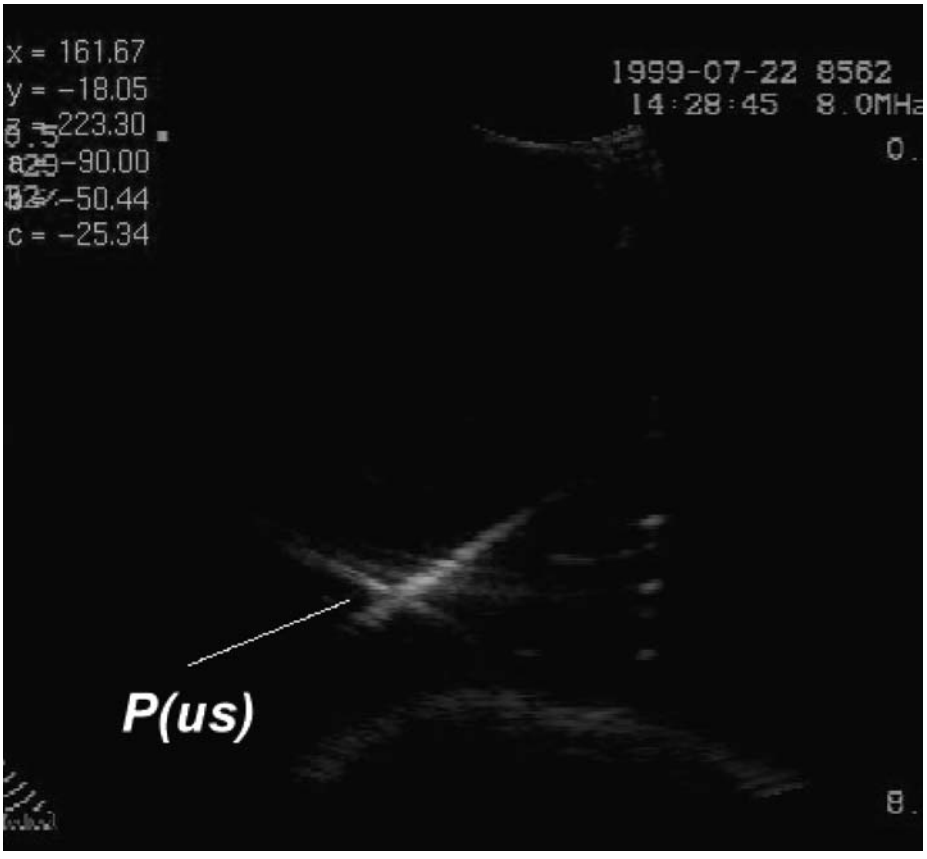

Fig. 2. Navigator screen-shot from the ultrasound window, depicting the target point ($\boldsymbol{P}_{US}$, star-like echo) together with the actual co-ordinates of the ultrasound probe tracking device (*TR CS*) as $X/Y/Z/$pitch$/$roll$/$yaw (upper left corner)

using COREL DRAW (version 8.0, Corel Corp., USA). For image scaling of the ultrasound image, the ultrasound calliper tool is used to quantify the pixel to mm ratio by measuring a physically defined object. A mm-to-pixel ratio of 0.267 mm/pixel was calculated. The 2D offset of the ultrasound image of the target $\boldsymbol{P}$ was measured in ultrasound image co-ordinates ($\boldsymbol{P}_{US}$ in US CS; X_{US}, Y_{US}, Z_{US} with $X_{US} = 0$). Interobserver reliability for target definition within 2-D ultrasound images was calculated from 30 images by two observers.

Calculation of the transformation for ultrasound calibration

The physical target $\boldsymbol{P}$ was imaged by the tracked ultrasound probe from three orthogonal directions (50 scans each) to maximize calibration accuracy. The scaled ultrasound image was depicted on the navigation screen along with the according probe-tracking co-ordinates (TR CS; X_{TR}, Y_{TR}, Z_{TR}, pitch_{TR} yaw_{TR}, roll_{TR}). Movement of the probe while scanning was excluded by a probe-support to exclude inaccuracies from latencies of synchronisation between ultrasound image and tracking coordinates. The calculation of the transformation for ultrasound image coordinates (US CS) to tracking coordinates (TR CS) within the navigation system (REF CS) is explained within the appendix.

Ultrasound image transfer, co-visualisation and visual test of fusion accuracy

The ultrasound image was transferred via a S-VHS video port/frame grabber to the navigational workstation. According to the spatial location and orientation of the actual 2-D-ultrasound scan, the preoperative imaging data (MR imaging or CT) was reformatted and displayed on the navigation screen (Fig. 3, lower left quadrant marked as "along 90°") along with the ultrasound image in real-time. Also, target contours defined preoperatively were overlaid onto the ultrasound image. Therefore, movement of the ultrasound probe resulted in real-time recalculation and visualization of an MR imaging or CT image plane along the identical spatial orientation as scanned by the ultrasound probe (Fig. 3).

The accuracy of integration of the 2-D-ultrasound image into the navigation was tested using a calibrated 3D-ultrasound phantom (M55 phantom, CIRS, VA, USA). The 3-D-phantom was scanned by MR imaging (Magnetom Vision, MPRAGE-Sequence, 1.25 mm slice thickness; German Cancer Research Centre, Heidelberg, Germany). Targets were contoured using the 3-D-data set imported into the neuronavigation workstation (ultrasound-to-MRI co-visualisation).

Results

Identification of optimal presets for ultrasound target localization

Digitally beam focusing sharpened the edges of the target image and broadened the range of gain intensity as ranked by the observers with best target clarity at 20%

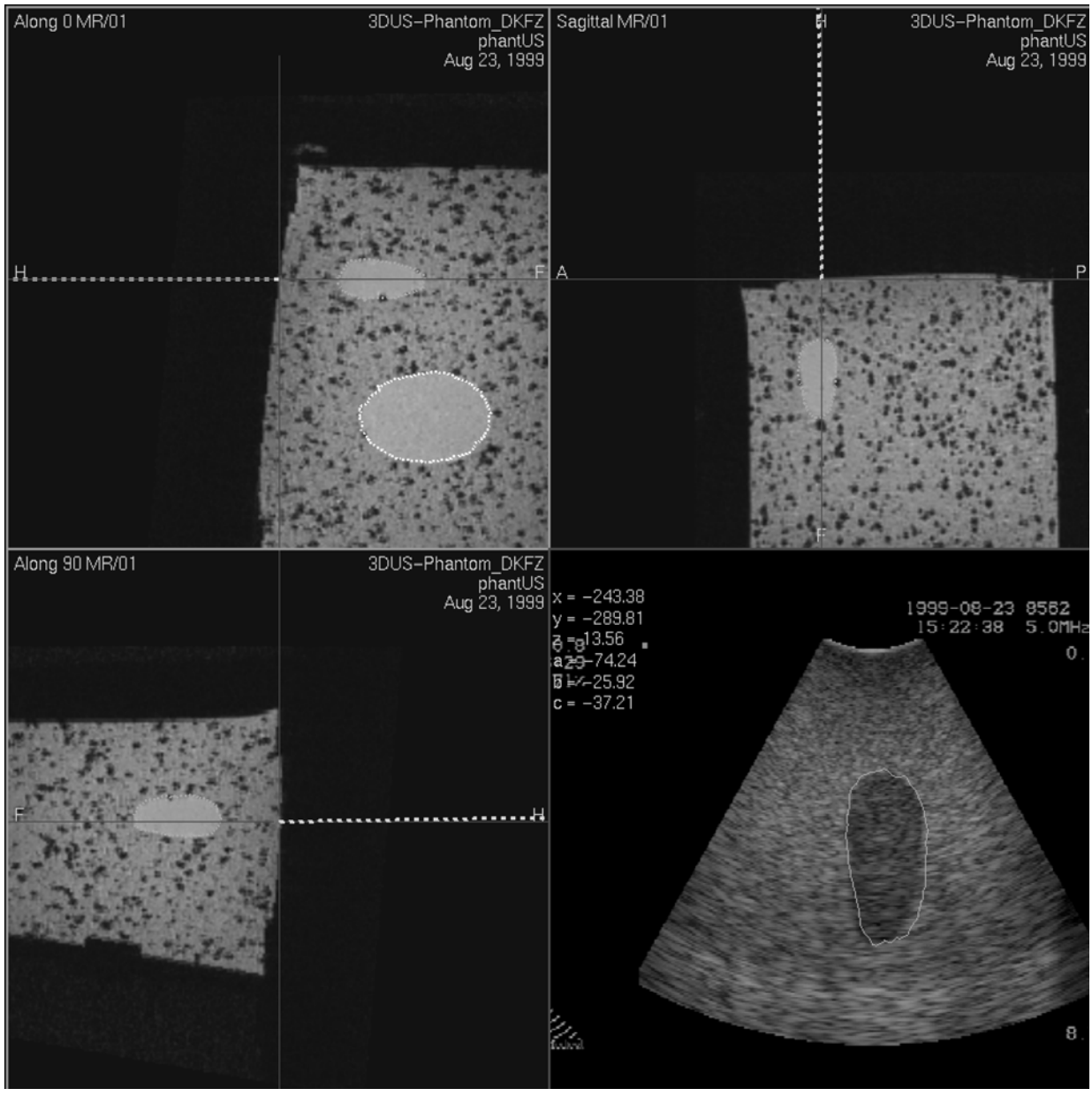

Fig. 3. Screen shot from the navigation screen (MR imaging of a 3-D ultrasound phantom). The navigated ultrasound image is seen on the lower right quadrant with accurately overlaid target contours derived from the reformatted MR image. The lower left quadrant depicts the reformatted MR image according to the ultrasound image localization and orientation within the reference co-ordinate system (*REF CS*). The dotted straight lines indicate the position of the ultrasound probe within the REF CS touching the surface of the phantom

gain intensity (Fig. 4). As a preset, gain intensity was set to 20% and digital beam focus was used in all calibration measurements.

Interobserver reliability of interactive target localization within the 2-D ultrasound image (US CS) was calculated from 30 images. Differences in target localization between two observers for Z_{US} and Y_{US} were -0.08 ± 0.32 mm and -0.39 ± 0.27 mm (mean $\pm$ SD), respectively. The interobserver error within the 2-D-area of the target was 0.5 ± 0.28 mm (mean $\pm$ SD). Regression coefficient for determination of the *Z*- and *Y*-co-ordinate was $r^2 = 0.990$ and $r^2 = 0.995$, respectively.

Registration and target localization

Target localization (definition of the crosshair of nylon threads, 50 measures, REF CS) using the navigational

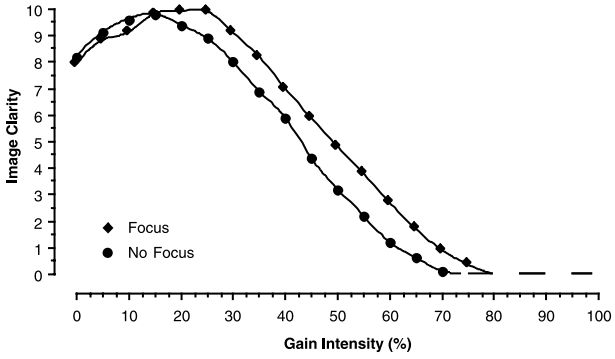

Fig. 4. Clarity of the target within the 2-D ultrasound image depending on gain intensity and digital beam focusing

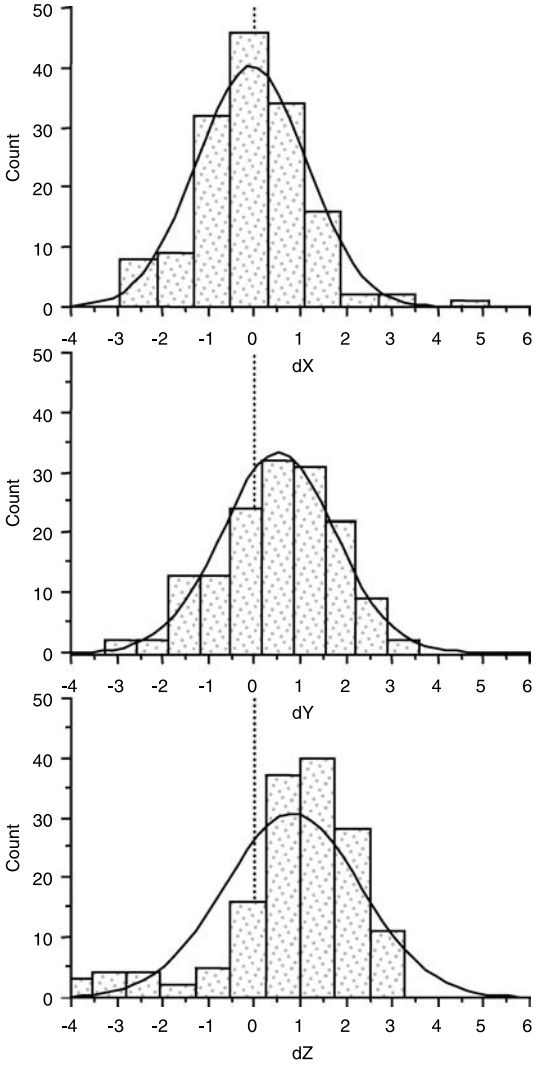

Fig. 5. Linear target localisation error of navigated ultrasound (Frequencies of deviation (d*X*, d*Y*, d*Z*) of the REF CS-transformed coordinates of $\boldsymbol{P}_{\mathrm{US}}$ from the physical target $\boldsymbol{P}_{\mathrm{REF}}$)

pointer under microscopic guidance was performed with a RMSE of 0.70 ± 0.23 mm (SD_X, 0.41 ± 0.17 mm; SD_Y, 0.40 ± 0.17 mm; SD_Z 0.38 ± 0.20 mm).

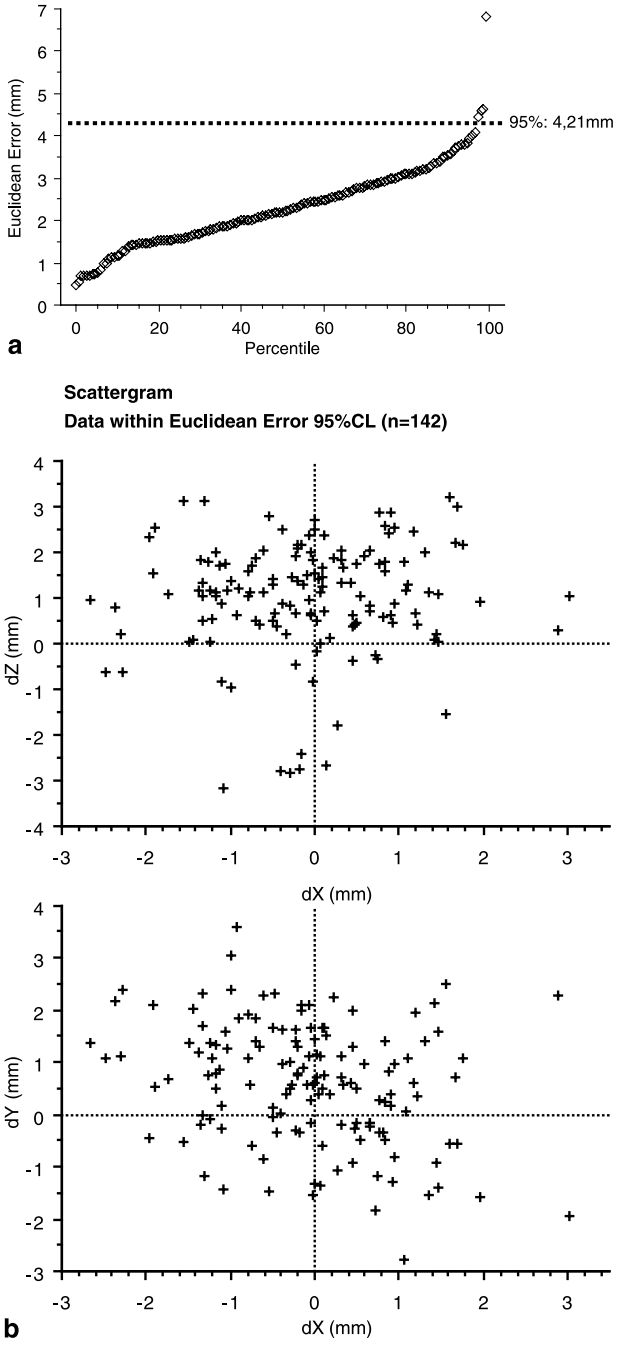

Fig. 6. (a) Target localisation error of navigated ultrasound: Euclidean error (Percentiles; deviation of the REF CS-transformed co-ordinates of $\boldsymbol{P}_{\mathrm{US}}$ from the physical target $\boldsymbol{P}_{\mathrm{REF}}$). (b) 95% confidence volume: Scattergram of linear target localisation errors (Deviation (d*X*, d*Y*, d*Z*) of the REF CS-transformed co-ordinates of $\boldsymbol{P}_{\mathrm{US}}$ from the physical target $\boldsymbol{P}_{\mathrm{REF}}$)

Target localization accuracy using navigated ultrasound

After calibration, ten different target points (crosshair of nylon threads) within the cross-wire phantom were tested. Each point in space was localized 10 to 20 times by navigated ultrasound. In total, 150 readings were available for analysis. Deviation of the target localization using ultrasound was best in the X_{REF}-orientation (-0.06 ± 1.19 mm; mean $\pm$ SD) and less precise in Y_{REF} and Z_{REF} direction (0.52 ± 1.23 mm and 0.83 ± 1.49 mm, respectively; Fig. 5). Mean overall LE (mean of ΔX_{REF}, ΔY_{REF} and ΔZ_{REF}) for target localization was 0.43 mm (SD: 1.36 mm; 95%CL: 3.13 mm). EE of target localization for each point in space is depicted in Fig. 6. The overall mean EE of all measures was 2.26 mm (SD: 0.97 mm; 95%CL: 4.21 mm).

Visual inspection of fusion accuracy between ultrasound and MRI

In the clinical situation, ultrasound-to-MRI fusion is displayed to the surgeon for augmented intraoperative orientation and was tested in addition. However, since registration of MR image data is one important source of error in this setting, localization accuracy of a physical target by navigated ultrasound is the most important accuracy (see above). Imaging of a 3-D ultrasound volume phantom revealed accurate integration of ultrasound into navigation for a volume target after registration (10 fiducials, REF CS registration error (RMSE): 1.8 mm). Target contours derived from the segmented MR imaging data were overlaid accurately onto the integrated ultrasound image in real-time (Fig. 3).

Discussion

Calibration accuracy of the integration of ultrasound into neuronavigation systems has been reported by some authors [9, 15, 17, 21]; however, most have focussed on preliminary clinical aspects.

The type of calibration phantom seems important. Prager *et al.* compared four different phantoms for calibration for 3-D ultrasound (single cross wire, three wires, single wall, Cambridge phantom). The single cross wire phantom used in our study revealed high accuracy and validity [19]. Two other groups reported about calibration accuracy using the cross wire phantom, both implementing magnetic digitiser based tracking systems [4, 9]. A localization error of 2.1 to 3.5 mm (RMSE, [4]) and 2.96 ± 1.85 mm (RMSE, mean $\pm$ SD; [9]) was reported. Using a LED-based navigation system, we achieved a better accuracy for the same type of phantom (mean EE: 2.26 mm; SD: 0.97 mm).

Hata *et al.* reported about two methods of ultrasound integration for brain surgery: integration of 2-D images into a 3-D MR image space by image matching, and frame based calibration with an accuracy of 3.5 mm [10]. They succeeded in co-visualization of ultrasound images fused with MR imaging, but both methods seemed not to be feasible under clinical routine conditions. For an optically tracked navigation system, an overall calibration accuracy of 4 mm was estimated using a multiple wire phantom as calibration target [23]. Using a volume phantom and interactive calibration, a target localization accuracy ranging 0.9 to 3.13 mm (mean: 1.3 mm) was reported for an arm based and an optical tracking system by Comeau and co-workers [3]. Gronningsaeter and coworkers (in [15]) reported an overall accuracy of ultrasound integration of their prototype of 2.7 mm with a potential for improvement to 1.7 mm. For the advanced system, a technical accuracy of 1.4 mm (arithmetic mean of the spatial error vector, standard deviation: 0.45 mm) has been reported recently in an extensive study by Lindseth [17]. These ranges of accuracy are in accordance with our findings and substantiate a technical basis for the integration of ultrasound into navigation regarding accuracy.

For clinical application, a spatial range of accuracy (with confidence limits) is at least as important as mean accuracies. 95% of all target points were localized within 4.21 mm distance from the actual target in our study (Fig. 6a). Improved accuracy was reported by Lindseth *et al.* [17] with a 95% confidence limit of 2.12 mm for 3D-ultrasound based navigation.

Sources of error

Resolution of ultrasound

For calibration purposes using a cross-wire phantom, ultrasound image resolution seems important. Axial resolution, i.e. distinction of targets along the ultrasound beam, lies within the sub millimetre range and depends on pulse duration and homogeneity of the phantom material (speed of sound). Scanning plane thickness determines the image dimension of least resolution in ultrasound. It depends mainly on probe geometry, gain intensity and depth of insonation. It ranges from nearly 1 mm [24] up to above 4 mm [9, 15] and may therefore disturb calibration accuracy. In their extensive study on calibration accuracy, Hartov *et al.* [9] did not comment

on their performance in target detection within the 2-D ultrasound image nor on specifications of the modalities (type of probe, frequency, gain intensity). These details seem important, because reduction of high or medium gain intensity to a subjectively optimal low gain reduces scanning plane thickness by 33% and 15%, respectively [25]. For the calibration process, high frequency and adequate low intensity gain along with digital beam focusing optimises image clarity and enables high inter-observer reliability for definition of the physical target ***P*** within US CS and for improvement of calibration accuracy. Technical improvements of the calibration accuracy have direct clinical implications, especially for 3D image reconstruction, since inaccuracies may add up during the process [17], and recently reported high accuracies seem sufficient for clinical application.

Even with optimised ultrasound settings, echogenic targets may be located slightly off the ideal scanning plane (at, above *or* below this plane) and slice thickness may cause inaccuracies at calibration. In our study the localizing error was prominent in the Y_{REF} and Z_{REF}. During validation, most ultrasound scans were made with the longitudinal ultrasound probe axis (Z_{US}) oriented along the X_{REF}. In this setting, highest image resolution is achieved in the X_{REF} direction while least image resolution (slice thickness error) either is oriented in Y_{REF} and Z_{REF} direction. As the ultrasound probe was moved freely within the navigation co-ordinate system, a quantitative distinction between errors along Y and Z axis cannot be given. This finding, however, does not support the theoretical presumption given by Hartov [9] that scanning plane error will tend to cancel with a high number of images. Instead, a bias during target identification on the 2-D ultrasound image perpendicular to the image plane may contribute to calibration inaccuracy. In contrast, Lindseth *et al.* [16] did not find any influence of image resolution on calibration accuracy using a membrane-based phantom. This is based on a 2D target, where identification of a point-like target is not necessary. This may explain why ultrasound image resolution seems be of less importance in their setting.

Lateral resolution is less important in calibration using a single target located within the focussed central beam area, but target delineation off the central beam may deteriorate target localization due to lateral resolution, especially with phased-array probes.

Probe calibration

Rigid coupling of the ultrasound probe to the localizing digitiser and phantom based calibration using the ultrasound image is the basis for successful integration of ultrasound into a navigation system.

Proper scaling of the ultrasound image is essential to calculate the target co-ordinates within the 2-D ultrasound co-ordinate system and the reference coordinate system. For image scaling of the ultrasound image, the ultrasound calliper tool is used to quantify the pixel to mm ratio by measuring a defined object. This source of error is negligible, because absolute image pixelation error of digital ultrasound calliper systems are 0.5 pixels in axial and lateral directions for phantom studies [7]. Target co-ordinates within the reference co-ordinate system were defined by a navigation pointer. Manual error of target definition by a pointer has been reported in the range of 1.36 mm (RMSE, [9]). Using a microscope-assisted procedure and a LED localizing system, we were able to refine this error down to 0.7 mm (RMSE). Further reduction of error in this setting seems only possible by non-contact measurement systems, e.g. laser.

A bias, i.e. offset of the mean of target points from zero, has also been reported by Gronningsaeter and co-workers (in [15]), but has not been adequately explained. In a very detailed accuracy study of 3D ultrasound based navigation, several factors affecting accuracy were identified and the problem of ultrasound scan thickness was discussed but not addressed [17]. This systematic error might be reduced by the elimination of manual error (i.e. human interaction) [15], e.g. by automatic target segmentation and multi-angle insonation during the calibration procedure, which is currently investigated. Also, a 2D-target-phantom might reduce its influence on calibration accuracy [16].

Speed of sound and synchronisation of US image to probe tracking coordinates

Phantom tests where performed in a water phantom and qualitatively validated using a tissue-mimicking phantom (M55, speed of sound: 1539 m/s). In the clinical setting, however, differences in speed of sound (SOS) between water (1480 m/s at 21 °C [24]) and brain tissue (1510 m/s) may lead to an additional error of axial distance of 2% along the ultrasound probe axis (X_{REF} in this in-vitro setting). This systematic error is clinically important and can be reduced by choosing a calibration phantom with adapted SOS or by correction for differences in SOS between the calibration phantom and the clinical target (depth dependent re-scaling of the reformatted MR image and overlaid contours).

Inaccuracy can occur due to improper temporal synchronisation of ultrasound probe co-ordinates and ultrasound image (delayed tagging of image and appropriate co-ordinates). Ultrasound image transfer to the navigation platform via S-VHS port/frame grabbing is prone to this error (approximately 200 ms delay) with a freely moving probe at the time of calibration. However, as the ultrasound probe was rigidly supported during calibration and validation, de-synchronisation is not likely to cause significant inaccuracy in our study. Exclusion of analogue image transfer by integration of the ultrasound platform into the navigation platform enables synchronized tagging and reduces this source of error. This problem was not addressed in this study.

We presented a calibration procedure for the integration of ultrasound images from an external ultrasound system into a navigation platform yielding a high target localization accuracy.

Conclusion

Integration of ultrasound images from an external ultrasound system into a neuronavigation platform can be achieved with a target localization accuracy of 2.26 mm (Euclidean error). This laboratory accuracy warrants studies on the clinical feasibility of this technique.

Disclosure

The authors have no financial interest in the system tested. This study was supported in part by the State Initiative "Hessen media", Ministry of Science and Art, State Government of Hesse, Germany.

Acknowledgment

We thank Dr. E. Herdt for technical and computational support. We thank the Department for Clinical and Administrative Data Processing at the University of Giessen (Head: Prof. Dr. K. Marquardt), Carl Zeiss Inc. and Leibinger Inc. for technical support. We are grateful to the Departments of Neuroradiology at the University of Giessen (Head: Prof. Dr. H. Traupe) and German Cancer Research Center/University of Heidelberg (Dr. Essig, Dr. Metzner) for providing image data. We are indebted to Dr. phil. nat. K. Seifert for technical advice.

Appendix

Calibration of the ultrasound probe is based on imaging a physical target $\boldsymbol{P}$ defined within the navigational co-ordinate system (CS). Four CS are linked for that purpose: The navigation camera defines the global co-ordinate system (GLOB CS), in which a reference frame (REF CS), rigidly linked to the cross-wire phantom, defines the physical target co-ordinates of $\boldsymbol{P}$. The tracked ultrasound probe (TR CS) is rigidly related to the ultrasound image (US CS), however, this relation is unknown (Fig. 1).

The CS are each pair-wise geometrically connected by a co-ordinate transformation ($M_{i,j}$) including a respective rotational and translational component, while scaling is absorbed by appropriately choosing the measurement conditions. This transformation $M_{i,j}$ transforms between the representation of the co-ordinates for any physical point. This also holds for a concatenation of three transformations $M_{\mathrm{REF,GLOB}}$, $M_{\mathrm{TR,US}}$, and $M_{\mathrm{GLOB,TR}}$ between the above mentioned CS US, TR, GLOB and REF. Different representations for such transformations $M_{i,j}$ exist. A four dimensional representation may be chosen in order to arive at a homogeneous transformation equation

$$\begin{aligned}\vec{p}_i &= M_{i,j}(t_x, t_y, t_z, \vartheta, \psi, \varphi) \circ \vec{p}_j \\ &= T(t_x, t_y, t_z) \circ R_z(\vartheta) \circ R_y(\psi) \circ R_x(\varphi) \circ \vec{p}_j \end{aligned} \quad (1)$$

for the co-ordinate transformation any two systems i and j wherein the rotational operations R_x, R_y, R_z as well as the translation operation T are four dimensional matrices and wherein $\vec{p}_j$ and $\vec{p}_i$ are four dimensional co-ordinate representations of the physical point $\boldsymbol{P}$.

It follows that the application of the concatenation of the transformations $M_{\mathrm{REF,GLOB}}$, $M_{\mathrm{GLOB,TR}}$ and $M_{\mathrm{TR,US}}$ to the representation $\vec{p}_{\mathrm{US}}$ of any physical point $\boldsymbol{P}$ in the US CS (ultrasound image) leads to the respective representation $\vec{p}_{\mathrm{REF}}$ of the same physical point $\boldsymbol{P}$ in the REF CS (phantom) according to the following equation:

$$\vec{p}_{\mathrm{REF}} = M_{\mathrm{REF,GLOB}} \circ M_{\mathrm{GLOB,TR}} \circ M_{\mathrm{TR,US}} \circ \vec{p}_{\mathrm{US}} \quad (2)$$

or

$$\begin{pmatrix} x_{\mathrm{REF}} \\ y_{\mathrm{REF}} \\ z_{\mathrm{REF}} \\ 1 \end{pmatrix} = M_{\mathrm{REF,GLOB}} \circ M_{\mathrm{GLOB,TR}} \circ M_{\mathrm{TR,US}} \circ \begin{pmatrix} x_{\mathrm{US}} \\ y_{\mathrm{US}} \\ z_{\mathrm{US}} \\ 1 \end{pmatrix}. \quad (3)$$

Thereby, the US co-ordinates of any physical point $\boldsymbol{P}$ can be connected to the reference (phantom) co-ordinates. The spatial relationship of the global system GLOB to the REF CS and TR CS- i.e. the operations $M_{\mathrm{REF,GLOB}}$ and $M_{\mathrm{GLOB,TR}}$ – have to be known or derived and $M_{\mathrm{TR,US}}$ is the unknown transformation. Based on repetitive measurements of physical points $\boldsymbol{P}$ the parameters for $M_{\mathrm{TR,US}}$ are calculated in order to minimize the error between the co-ordinates of $\boldsymbol{P}$ measured directly in REF CS and $\boldsymbol{P}$ imaged by ultrasound in REF CS after transformation from US CS according to Eq. (3).

The translational transformation $T(t_x, t_y, t_z)$ and the rotational operations $R_z(\vartheta), R_y(\psi), R_x(\varphi)$ in the four dimensional representation are in each case of the transformations US $\rightarrow$ TR, TR $\rightarrow$ GLOB, GLOB $\rightarrow$ REF given by:

$$T(t_x, t_y, t_z) = \begin{pmatrix} 1 & 0 & 0 & t_x \\ 0 & 1 & 0 & t_y \\ 0 & 0 & 1 & t_z \\ 0 & 0 & 0 & 1 \end{pmatrix} \text{ and e.g. by}$$

$$R_x(\varphi) = \begin{pmatrix} \cos(\varphi) & \sin(\varphi) & 0 & 0 \\ -\sin(\varphi) & \cos(\varphi) & 0 & 0 \\ 0 & 0 & 1 & 0 \\ 0 & 0 & 0 & 1 \end{pmatrix} \quad (4)$$

and for $R_y(\psi)$ and for $R_z(\vartheta)$ similar relations holds [2].

In general, most of the transformation parameters φ, ψ, and ϑ as well as t_x, t_y, and t_z are a priori unknown and have to be derived. The calibration obtains the parameters for $M_{\mathrm{TR,US}}$ by repetitive measurements for a particular high degree of accuracy. Therefore, 150 measurements of $\boldsymbol{P}$ were performed to reduce scatter around the target and statistical errors. An iterative algorithm was chosen related to Detmer *et al.* [4]. Meanwhile, a distinct mathematical solution for transformation calculation has been derived and published [9]. The resulting transformation was integrated into the STP-navigation software. Target localization error of $\boldsymbol{P}$ by navigation-integrated ultrasonography was calculated as linear error (LE) for X, Y and Z in REF CS as well as Euclidean error (EE; [5]):

$$\mathrm{EE} = \sqrt{\Delta x^2 + \Delta y^2 + \Delta z^2} \quad (5)$$

with $\Delta X = X(P_{\mathrm{REF}}) - X(P_{\mathrm{US}} \circ M_{\mathrm{REF,GLOB}} \circ M_{\mathrm{GLOB,TR}} \circ M_{\mathrm{TR,US}})$ and according notations for Y and Z.

References

1. Black PM, Moriarty T, Alexander 3rd E, Stieg P, Woodard EJ, Gleason PL, Martin CH, Kikinis R, Schwartz RB, Jolesz FA (1997) Development and implementation of intraoperative magnetic resonance imaging and its neurosurgical applications. Neurosurgery 41: 831–842
2. Bronstein I, Semendjajew K, Musiol G, Mühling H (1998) Taschenbuch der Mathematik. Verlag Harri Deutsch p 204–222, 250–257
3. Comeau R, Sadikot A, Fenster A, Peters T (2000) Intraoperative ultrasound for guidance and tissue shift correction in image-guided neurosurgery. Med Phys 27: 787–800
4. Detmer PR, Bashein G, Hodges T, Beach KW, Filer EP, Burns DH, Strandness DE Jr (1994) 3D ultrasonic image feature localization based on magnetic scanhead tracking: in vitro calibration and validation. Ultrasound Med Biol 20: 923–936
5. Dorward NL, Alberti O, Palmer JD, Kitchen ND, Thomas DG (1999) Accuracy of true frameless stereotaxy: in vivo measurement and laboratory phantom studies. Technical note. J Neurosurg 90: 160–168
6. Dorward NL, Alberti O, Velani B, Gerritsen FA, Harkness WF, Kitchen ND, Thomas DG (1998) Postimaging brain distorsion: magnitude, correlates, and impact on neuronavigation. J Neurosurg 88: 656–662
7. Goldstein A (2000) Errors in ultrasound digital image distance measurement. Ultrasound Med Biol 26: 1125–1132
8. Gronningsaeter A, Kleven A, Ommendal S, Aarseth T, Lindseth F, Lango T, Unsgard G (2000) SonoWand, an ultrasound-based neuronavigation system. Neurosurg 47: 1373–1380
9. Hartov A, Eisner SD, Roberts DW, Paulsen KD, Platenik LA, Miga MI (1999) Error analysis for a free-hand three-dimensional ultrasound system for neuronavigation. Neurosurgical Focus 6: Article 5
10. Hata N, Dohi T, Iseki H, Takakura K (1997) Development of a frameless and armless stereotactic neuronavigation system with ultrasonographic registration. Neurosurgery 41: 608–613
11. Hill DL, Maurer CR Jr, Maciunas RJ, Barwise JA, Fitzpatrick JM, Wang MY (1998) Measurement of intraoperative brain surface deformation under a craniotomy. Neurosurgery 43: 514–526
12. Hirschberg H, Unsgaard G (1997) Incorporation of ultrasonic imaging in an optically coupled frameless stereotactic system. Acta Neurochir (Wien) [Suppl] 68: 75–80
13. Jödicke A, Deinsberger W, Erbe H, Kriete A, Böker DK (1998) Intraoperative three-dimensional ultrasonography: an approach to register brain shift using multidimensional image processing. Minim Invasive Neurosurg 41: 13–19
14. Koivukangas J, Kelly PJ (1986) Application of ultrasound imaging to stereotactic brain tumor surgery. Ann Clin Res 18: 25–32
15. Lango T (2001) Ultrasound guided surgery: image processing and navigation. Department of Ultrasound, SINTEF Unimed. Norwegian University of Science and Technology, Trondheim (Thesis)
16. Lindseth F, Bang J, Lango T (2003) A robust and automatic method for evaluating accuracy in 3-D ultrasound-based navigation. Ultrasound in Med & Biol 29: 1439–1452
17. Lindseth F, Lango T, Bang J, Nagelhus Hernes T (2002) Accuracy evaluation of a 3D ultrasound-based neuronavigation system. Comp Aid Surg 7: 197–222
18. Nabavi A, Black PM, Gering DT, Westin C-F, Metha V, Pergolizzi RSJ, Ferrant M, Warfield SK, Hata N, Schwartz RB, Wells WM, Kikinis R, Jolesz FA (2001) Serial intraoperative magnetic resonance imaging of brain shift. Neurosurgery 48: 787–798
19. Prager RW, Rohling RN, Gee AH, Berman L (1998) Rapid calibration for 3-D freehand ultrasound. Ultrasound Med Biol 24: 855–869
20. Roberts DW, Hartov A, Kennedy FE, Miga MI, Paulsen KD (1998) Intraoperative brain shift and deformation: a quantitative analysis of cortical displacement in 28 cases. Neurosurgery 43: 749–760
21. Trobaugh JW, Richard WD, Smith KR, Bucholz RD (1994) Frameless stereotactic ultrasonography: method and applications. Comput Med Imaging Graph 18: 235–246
22. Tronnier VM, Wirtz CR, Knauth M, Lenz G, Pastyr O, Bonsanto MM, Albert FK, Kuth R, Staubert A, Schlegel W, Sartor K, Kunze S (1997) Intraoperative diagnostic and interventional magnetic resonance imaging in neurosurgery. Neurosurgery 40: 891–900
23. Vince G, Woydt M, Witte J, Horowski A, Roosen K, Krone A (1999) Real-time ultrasound fusion in CT/MR image-guided surgery. J Neurosurg 90: 422 (abstract)
24. Zagzebski J (1996) Essentials in ultrasound physics. Mosby, St. Louis
25. Zdero R, Fenton P, Bryant J (2002) A digital image analysis method for diagnostic ultrasound calibration. Ultrasonics 39: 695–702

Comments

Jödicke and colleagues report their development of a system in which ultrasound imaging is co-registered with their image-guidance system. Their methodology of calibrating the ultrasound probe and their experience using this system with a phantom target are presented along with optimised ultra-sound presets under these conditions. Very accurate results for target localization are reported.

The system and methodology described in this technical note are sound. The topic is of moderate relevance to the field of image-guided surgery. Similar work has already been published by a number of groups. However, and this somewhat diminishes excitement for its findings.

David W. Roberts

This paper describes the integration of real-time 2D ultrasound into a traditional navigation system based on preoperative data. A commercial ultrasound system is linked to a commercial navigation system using video grabbing. The ultrasound probe is calibrated and the ultrasound target localization accuracy is tested using a phantom in a laboratory setting. This could be a feasible approach for the many institutions that have both a navigation system and an ultrasound scanner, in order to achieve intra-operate imaging. The authors address the accuracy that can be achieved by such a system and as such this is an important paper and a valid contribution to the field.

Geirmund Unsgaard and *Frank Linseth*
Trondheim

Correspondence: A. Jödicke, MD, Department of Neurosurgery, University Medical Centre, Justus-Liebig-Universität, Klinikstr. 29, 35385 Giessen, Germany. e-mail: andreas.joedicke@neuro.med.uni-giessen.de